Journal of Quantitative Spectroscopy & Radiative Transfer 112 (2011) 1726–1732

Contents lists available at ScienceDirect

Journal of Quantitative Spectroscopy & Radiative Transfer

journal homepage: www.elsevier.com/locate/jqsrt

T-matrix approach to calculating circular polarization of aggregates made of optically active materials

D. Mackowski [a,*], L. Kolokolova [b], W. Sparks [c]

[a] Department of Mechanical Engineering, Auburn University, Auburn, AL, USA
[b] Department of Astronomy, University of Maryland, College Park, MD, USA
[c] Space Telescope Science Institute, Baltimore, MD, USA

ARTICLE INFO

Available online 15 February 2011

Keywords:
Aggregate scattering
Circular polarization
Optically active

ABSTRACT

Optical activity is a typical property of the biological materials where left-handed amino-acids and right-handed carbohydrates dominate (so called homochirality). Observationally, optically active materials reveal themselves through the circular polarization in the light they scatter. Thus, circular polarization produced by the optically active particles can serve as a biomarker. It is known that biological (e.g. colonies of bacteria) and pre-biological (e.g. dust in comets) particles often have a complex structure that can be modeled presenting them as aggregates of small monomers. This motivated the development of the *T*-matrix code presented in this paper, which enables calculation of the scattering matrix – including circular polarization – of the light scattered by aggregated optically active particles. The code can be used for modeling the light scattering by biological objects (e.g. colonies of bacteria, blood cells) and for interpretation of the circular polarization produced by the cosmic dust that contains (pre)biological organic, e.g. comet dust or planetary aerosols.

1. Introduction

Many complex organic molecules exist in two forms that are identical except that they pose chirality, i.e., are mirror images of each other. A typical characteristic of life is the homochirality of biological molecules, i.e., predominance of one of the mirror forms of the organic molecules. This characteristic may be manifested on a macroscopic scale through the optical activity of the chiral molecules and, hence, the presence of circular polarization (CP) in the light they scatter. Recently a set of data on circular polarization in comets has been accumulated [1,2]. Characteristics of the cometary CP in the set, specifically an average toward left-handed polarization, could be viewed as evidence of homochiral organics in comet dust similar to that found in meteorites [3]. We have also explored remote sensing capabilities of circular polarization in the laboratory, by studying light scattering from astrobiologically relevant microorganisms and setting these in the context of abiotic minerals [4]. We have found a dependence of the CP on the dichroism of the materials that results in greater circular polarization in absorption bands.

Theoretical and computational tools are needed to confirm whether the presence of chiral organics can produce the observed characteristics of comet circular polarization and explain the results of our laboratory measurements. A well known solution exists for an isolated, optically active sphere [5], yet a single-sphere model for complex comet dust particles or colonies of bacteria is both unrealistic and incapable of explaining recent results.

A significant part of comet dust is in the form of particles having an aggregated structure [6], and such a structure is also plausible for a variety of biological

* Corresponding author. Tel.: +13348443334; fax: +13348443307.
E-mail address: mackodw@auburn.edu (D. Mackowski).

0022-4073/$ - see front matter © 2011 Elsevier Ltd. All rights reserved.
doi:10.1016/j.jqsrt.2011.02.003

particles. To better account for the non-spherical nature of such particles, we have developed a *T*-matrix code to predict light scattering and absorption by aggregates of optically active (OA) spheres. We anticipate that this code will be applicable to a variety of astrobiological problems, including the search for materials containing molecules of pre-biological and biological origin in comets, planets, extrasolar planets, and protoplanetary nebulae as well as for studying biological particles in the Earth atmosphere and in the laboratory.

The paper will present the formulation and computational algorithm for calculating the *T*-matrix for a cluster of OA spheres. As will be shown, the solution can predict the detailed electromagnetic field both within and external to the spheres, and we use this capability in example calculations to demonstrate the veracity of the code. We also present a limited set of calculations that show the effects of OA on circular polarization of aggregated particles.

2. Formulation

The formulation for interactive scattering among a cluster of optically active spheres can be obtained by a merging of the formulations for optically active single spheres and multiple, non-active spheres. We will begin by reviewing the single (or isolated) sphere relations, and then describe the required modifications to the interacting sphere formulation that are needed to account for optical activity.

2.1. The T-matrix for a single OA sphere

The defining characteristic of OA media is that only circularly polarized, homogenous plane waves can propagate in such media without undergoing a change in polarization state. Following the formulation of Bohren and Huffman [7], the electric and magnetic fields propagating within OA media can be constructed from a linear transformation of left and right expansion functions [7], denoted as Q_L and Q_R, i.e.,

$$\begin{pmatrix}\mathbf{E}\\ \mathbf{H}\end{pmatrix}=\mathbf{A}\begin{pmatrix}\mathbf{Q}_L\\ \mathbf{Q}_R\end{pmatrix} \tag{1}$$

in which the matrix $\mathbf{A}$ is

$$\mathbf{A}=\begin{pmatrix}1 & -\mathrm{i}/\mathrm{m}\\ -\mathrm{i}\mathrm{m} & 1\end{pmatrix} \tag{2}$$

The $\mathbf{Q}$ expansion functions satisfy

$$\nabla\times\mathbf{Q}_L=k_L\mathbf{Q}_L \tag{3}$$

$$\nabla\times\mathbf{Q}_R=-k_R\mathbf{Q}_R \tag{4}$$

in which $k_L=2\pi\mathrm{m}_L/\lambda$ and $k_R=2\pi\mathrm{m}_R/\lambda$ are the left and right wavenumbers for the medium, with m_L and m_R denoting the relative refractive indices for left and right circularly polarized light. The left and right refractive indices are related to the average (or bulk) refractive index m by

$$\mathrm{m}=\frac{2}{1/\mathrm{m}_L+1/\mathrm{m}_R} \tag{5}$$

In addition, the left and right refractive indices can be specified by the average m and a complex chiral factor β by

$$\mathrm{m}_L=\frac{\mathrm{m}}{1-\beta\mathrm{m}},\quad \mathrm{m}_R=\frac{\mathrm{m}}{1+\beta\mathrm{m}} \tag{6}$$

The $\mathbf{Q}$ expansion functions can be represented in the interior of an OA sphere by expansions of the regular vector wave harmonics (VWH) $\mathbf{N}^{(1)}_{mnp}(k\mathbf{r})$, of order n, degree m, and mode p=1 (TM) or 2 (TE). The VWHs satisfy the vector Helmholtz equation

$$\nabla^2\mathbf{N}^{(1)}_{mnp}(k\mathbf{r})+k^2\mathbf{N}^{(1)}_{mnp}(k\mathbf{r})=0 \tag{7}$$

as well as

$$\nabla\times\mathbf{N}^{(1)}_{mn1}(k\mathbf{r})=k\mathbf{N}^{(1)}_{mn2}(k\mathbf{r}),\quad \nabla\times\mathbf{N}^{(1)}_{mn2}(k\mathbf{r})=k\mathbf{N}^{(1)}_{mn1}(k\mathbf{r}) \tag{8}$$

With this set of basis functions, formulas for the $\mathbf{Q}$ expansion functions will appear as

$$\mathbf{Q}_L(\mathbf{r})=\sum_{n=1}\sum_{m=-n}^{n}c_{mnL}(\mathbf{N}^{(1)}_{mn1}(k_L\mathbf{r})+\mathbf{N}^{(1)}_{mn2}(k_L\mathbf{r})) \tag{9}$$

$$\mathbf{Q}_R(\mathbf{r})=\sum_{n=1}\sum_{m=-n}^{n}c_{mnR}(\mathbf{N}^{(1)}_{mn1}(k_R\mathbf{r})-\mathbf{N}^{(1)}_{mn2}(k_R\mathbf{r})) \tag{10}$$

in which c_{mnL} and c_{mnR} denote the sought expansion coefficients for the internal field.

Exterior to the sphere, the incident and scattered fields will be represented by the usual expansions of regular and outgoing VWH, i.e.,

$$\mathbf{E}_{inc}(\mathbf{r})=\sum_{n=1}\sum_{m=-n}^{n}\sum_{p=1}^{2}f_{mnp}\mathbf{N}^{(1)}_{mnp}(k\mathbf{r}) \tag{11}$$

$$\mathbf{E}_{sca}(\mathbf{r})=\sum_{n=1}\sum_{m=-n}^{n}\sum_{p=1}^{2}a_{mnp}\mathbf{N}^{(3)}_{mnp}(k\mathbf{r}) \tag{12}$$

in which the expansion coefficients f for the incident field will depend on the direction and polarization state of the field. Evaluation of the continuity conditions at the sphere surface will yield a linear relation between the scattering and incident field coefficients, of the form

$$a_{mnp}=\sum_{q=1}^{2}\overline{a}_{n;pq}f_{mnq} \tag{13}$$

in which the coefficients $\overline{a}$ will be a function of the sphere size parameter ka and the left and right refractive indices. These are analogous to the Lorenz–Mie coefficients for non-active spheres. Explicit formulas are

$$\overline{a}_{n;11}=-\frac{V_n(L)A_n(R)+V_n(R)A_n(L)}{D_n} \tag{14}$$

$$\overline{a}_{n;22}=-\frac{W_n(L)B_n(R)+W_n(R)B_n(L)}{D_n} \tag{15}$$

$$\overline{a}_{n;12}=\overline{a}_{n;21}=\frac{W_n(L)A_n(R)+W_n(R)A_n(L)}{D_n} \tag{16}$$

$$D_n=W_n(L)V_n(R)+W_n(R)V_n(L) \tag{17}$$

$$W_n(J)=-(\xi_n(x)\psi'_n(x\mathrm{m}_J))+\mathrm{m}\psi_n(x\mathrm{m}_J)\xi'_n(x) \tag{18}$$

$$V_n(J)=-(\mathrm{m}\xi_n(x)\psi'_n(x\mathrm{m}_J))+\psi_n(x\mathrm{m}_J)\xi'_n(x) \tag{19}$$

$$A_n(J) = \mathrm{m}\psi_n(x\mathrm{m}_J)\psi'_n(x) - \psi_n(x)\psi'_n(x\mathrm{m}_J) \tag{20}$$

$$B_n(J) = \psi_n(x\mathrm{m}_J)\psi'_n(x) - \mathrm{m}\psi_n(x)\psi'_n(x\mathrm{m}_J) \tag{21}$$

in which ψ_n and ξ_n denote the Ricati–Bessel and Ricati–Hankel functions. The coefficients for the internal fields can be related to the scattering coefficients, again by application of the surface continuity conditions. The formulas are

$$c_{nmL} = \overline{c}_{n;L1}a_{mn1} + \overline{c}_{n;L2}a_{mn2} \tag{22}$$

$$c_{nmR} = \overline{c}_{n;R1}a_{mn1} + \overline{c}_{n;R2}a_{mn2} \tag{23}$$

$$\overline{c}_{n;L1} = -\frac{\mathrm{i}\mathrm{m}_L B_n(R)}{F_n} \tag{24}$$

$$\overline{c}_{n;L2} = -\frac{\mathrm{i}\mathrm{m}_L A_n(R)}{F_n} \tag{25}$$

$$\overline{c}_{n;R1} = \frac{\mathrm{m}_R \mathrm{m} B_n(L)}{F_n} \tag{26}$$

$$\overline{c}_{n;R2} = -\frac{\mathrm{m}_R \mathrm{m} A_n(L)}{F_n} \tag{27}$$

$$F_n = A_n(L)B_n(R) + A_n(R)B_n(L) \tag{28}$$

The most salient feature of the single-sphere formulation, with respect to the extension of the formulation to multiple spheres, is that the single-sphere TE and TM modes are coupled for optically active spheres. That is, a TM mode incident field excitation will produce a TE mode scattering component, and visa-versa. This is in contrast to Lorenz–Mie scattering, for which the excitation and scattering modes are uncoupled.

2.2. Extension to multiple OA spheres

The formulation for scattering by neighboring spheres is made only marginally more complicated by optical activity of the spheres. This formulation represents the field external to the spheres by the superposition of the incident field and the fields scattered from each sphere in the ensemble:

$$\mathbf{E}_{ext} = \mathbf{E}_{inc} + \mathbf{E}_{sca} = \mathbf{E}_{inc} + \sum_{i=1}^{N_S} \mathbf{E}_{sca,i} \tag{29}$$

As was done for the single-sphere problem, the incident and scattered fields, at the ith sphere in the cluster, can be represented by regular and outgoing vector spherical harmonic (VWH) expansions, centered about the origin of the sphere:

$$\mathbf{E}_{inc} = \sum_{n=1}^{L_i}\sum_{m=-n}^{n}\sum_{p=1}^{2} f^i_{mnp}\mathbf{N}^{(1)}_{mnp}(\mathbf{r}-\mathbf{r}_i) \tag{30}$$

$$\mathbf{E}_{sca,i} = \sum_{n=1}^{L_i}\sum_{m=-n}^{n}\sum_{p=1}^{2} a^i_{mnp}\mathbf{N}^{(3)}_{mnp}(\mathbf{r}-\mathbf{r}_i) \tag{31}$$

in which L_i denotes the truncation order of the expansions.

The exciting field at the surface of a particular sphere, say sphere i, consists of the incident field plus the fields scattered from all other spheres in the cluster. This latter component can be represented by a regular VWH expansion by application of the addition theorem for vector harmonics. And the exciting field can be linearly related to the scattered field from the sphere by application of the optically active sphere T-matrix relation in Eq. (13). The end result is a set linear equations for the scattering coefficients,

$$a^i_{mnp} - \sum_{p'=1}^{2}\overline{a}^i_{n;pp'}\sum_{\substack{j=1\\ j\neq i}}^{N_S}\sum_{l=1}^{L_j}\sum_{k=-l}^{l}\sum_{q=1}^{2} H^{i-j}_{mnpklq}a^j_{klq} = \sum_{p'=1}^{2}\overline{a}^i_{n;pp'}f^i_{mnp'} \tag{32}$$

In the above H^{i-j} is an outgoing harmonic translation matrix, and depends solely on the distance and direction between origins i and j.

Following solution of Eq. (32) for a given incident state, the scattered field from the cluster can be represented via the superposition of Eq. (29), although this form must explicitly take into account the different phase lags between the spheres. Alternatively, the scattered field from the cluster can be represented by a single outgoing VWH expansion, centered about a common origin of the cluster, by application of the translation operations to the individual expansion in Eq. (31). This results in

$$\mathbf{E}_{sca} = \sum_{n=1}^{L}\sum_{m=-n}^{n}\sum_{p=1}^{2} a_{mnp}\mathbf{N}^{(3)}_{mnp}(\mathbf{r}) \tag{33}$$

$$a_{mnp} = \sum_{i=1}^{N_S}\sum_{l=1}^{L}\sum_{k=-l}^{l}\sum_{q=1}^{2} J^{0-i}_{mnpklq}a^i_{klq} \tag{34}$$

in which J is the regular harmonic translation matrix. The amplitude and scattering matrix elements for the cluster can be obtained from the standard formulas applied to the coefficients in Eq. (33) [7,8].

It will be shown in the following section that a highly accurate method for computing the orientation-averaged scattering matrix values of OA aggregates will be required to distinguish between the effects, on circular polarization, of geometrical structure and optical activity. And in this regard the superposition T-matrix method (STMM), with its associated analytical orientation averaging capability, will be the most efficient and accurate method to obtaining orientation-averaged scattering matrix values for OA aggregates. The T-matrix for the aggregate is defined so that

$$a_{mnp} = \sum_{l=1}^{L}\sum_{k=-l}^{l}\sum_{q=1}^{2} T_{mnpklq}f_{klq} \tag{35}$$

in which a_{mnp} are the cluster-centered expansion coefficients appearing in Eq. (34), f_{klq} are the coefficients of the regular VWH expansion, centered about the cluster origin, for the incident field, and L is an overall order limit for the cluster-based expansions. The cluster-based incident field coefficients can be related to those centered about a sphere origin i, as appearing in Eq. (30), by application

of the VWH translation operation

$$f^i_{mnp} = \sum_{l=1}^{L} \sum_{k=-l}^{l} \sum_{q=1}^{2} J^{i-0}_{mnpklq} f_{klq} \tag{36}$$

By using Eq. (36) in (32), the cluster T-matrix can be shown to be [8]

$$T_{mnpklq} = \sum_{i=1}^{N_S} \sum_{n'=1}^{L} \sum_{m'=-n'}^{n'} \sum_{p'=1}^{2} J^{0-i}_{mnpm'n'p'} T^i_{m'n'p'klq} \tag{37}$$

in which the sphere-cluster T^i matrices satisfy

$$T^i_{mnpklq} - \sum_{p'=1}^{2} \overline{a}^i_{n;pp'} \sum_{\substack{j=1 \\ j\neq i}}^{N_S} \sum_{l'=1}^{L_j} \sum_{k'=-l'}^{l'} \sum_{q'=1}^{2} H^{i-j}_{mnpk'l'q'} T^j_{k'l'q'klq} = \sum_{p'=1}^{2} \overline{a}^i_{n;pp'} J^{i-0}_{mnp'klq} \tag{38}$$

The computational algorithm for calculation of the cluster T-matrix iteratively solves Eq. (38) for the sequence $l=1,2,\ldots$, $k=-l, -l+1,\ldots l$, $q=1,2$. Following each solution the column elements of T are obtained from Eq. (37).

The orientation-averaged cross sections of the cluster can be identified by multiplication of Eq. (38) by $T^{i*}\overline{b}^i$, in which

$$\overline{b}_{n;pp'} = \overline{\mathbf{a}}^{-1}_n = (-1)^{p+p'} \frac{\overline{a}_{n;(3-p)(3-p)}}{\overline{a}_{n;11}\overline{a}_{n;22} - \overline{a}^2_{n;12}} \tag{39}$$

and contracting over m,n,p. By using the properties of the translation matrices, it can be shown that

$$\langle C_{abs} \rangle + \langle C_{sca} \rangle = \langle C_{ext} \rangle \tag{40}$$

$$\langle C_{abs} \rangle = -\frac{2\pi}{k^2} \mathrm{Re} \sum_{i=1}^{N_S} \sum_{n,m} \sum_{p,p'} \sum_{l,k,q} T^{i*}_{mnpklq} (\overline{b}_{n;pp'} + \delta_{p-p'}) T^i_{mnp'klq} \tag{41}$$

$$\langle C_{sca} \rangle = \frac{2\pi}{k^2} \sum_{n,m,p} \sum_{l,k,q} |T_{mnpklq}|^2 \tag{42}$$

$$\langle C_{ext} \rangle = -\frac{2\pi}{k^2} \mathrm{Re} \sum_{n,m,p} T_{mnpmnp} \tag{43}$$

With the exception of that for the absorption cross sections, these formulas are identical to those for clusters of isotropic spheres. The formulas for the orientation-averaged scattering matrix – which involve products of the T-matrix – will also be unchanged from the isotropic case [8].

2.3. Coding aspects

The OA multiple sphere formulation has been developed into a conventional (i.e., serial) code using the FORTRAN-90 programming language. In general, for N_S spheres with equal size parameters of x_S, and a corresponding sphere-level harmonic order limit of $L_S \sim x_S$, the memory requirements of the code will scale as $N_S L_S^3$ and the time required for a single solution to Eq. (38) will scale as $N_S^2 L_S^4$. Calculation of the T-matrix requires on the order of L^2 solutions to Eq. (38), in which $L \sim x_C$ where x_C is the size parameter of the circumscribing sphere for the cluster. In view of these factors, the serial code – which would typically run on conventional desktop or laptop PCs having a few GB of memory – is practical for T-matrix calculations of clusters containing up to a few hundred order-unity size parameter spheres. We have recently developed a parallel version of the code, which uses message passing interface (MPI) instructions and is designed for distributed memory compute clusters [9]. We anticipate that the parallel code will make practical random-orientation scattering property calculation of clusters containing several thousand spheres.

A number of consistency checks have been applied to test the veracity of the solution for clusters of optically active spheres. The results identically satisfy energy conservation (extinction = absorption + scattering), and they conform to equivalent rotations of the cluster and the incident field. In addition, the solution provides a detailed prediction of the electric field in the near-field zones – both within and exterior to the spheres – and this can be used to check the continuity conditions at the surfaces of the spheres. Also, for a single sphere, the solution reduces to the solution from [5] and for isotropic material it provides the standard multi-sphere case from [8].

Results shown in Figs. 1 and 2 demonstrate the veracity of the formulation as a solution to the boundary value problem. The results correspond to a cluster of four identical touching spheres arranged in a square pattern. The size parameter of the spheres is x=8 and the mean refractive index is m=1.55. Shown in Fig. 1 are contour

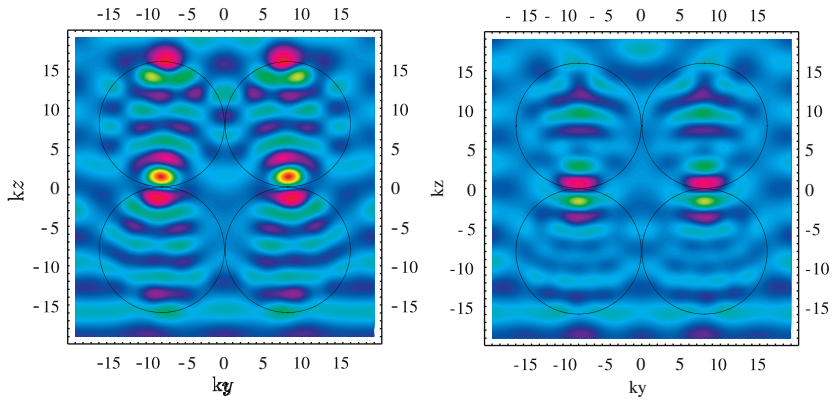

Fig. 1. Contour plots of normal electric field component. Propagation direction is upwards, polarization is normal.

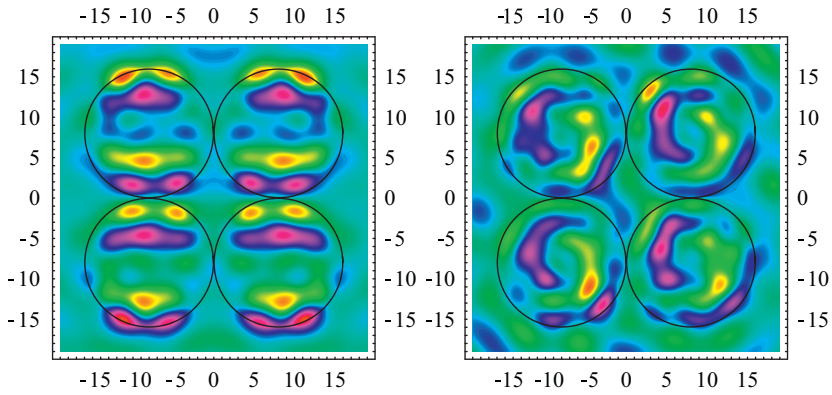

Fig. 2. Contour plots of normal electric field component. Propagation direction is into paper, polarization is upwards.

plots of the x-component of electric field (normal to the paper) for an x-polarized incident field propagating in the z direction (tangential to the paper, and upwards). The plot on the left has $\beta = 0$ (i.e., non-active spheres) and on the right $\beta = 0.1$.

The plots show the required continuity of the electric field at the sphere boundaries: the plotting plane intersects the sphere equator, and the plotted electric field is normal to this plane. Therefore, the plotted component of electric field is tangential to the sphere surface at the boundaries, and this component must be continuous. There is an effect of activity on the field patterns, yet the active case does not break the symmetry of the field patterns. This would be expected for the particular plotting conditions; optical activity will alter the coupling among the spheres, yet for this particular case the coupling will be symmetric, i.e., the spheres on the left will affect those on the right in the same way as right affects left.

The results in Fig. 2 show the same cluster configuration, except this time the propagation direction is into the paper, and the incident electric field vector is tangential to the paper and pointed upwards. The plot shows the normal component of the electric field, except this time the normal component does not include the incident field vector. Nevertheless, the continuity conditions at the surfaces are maintained. This configuration does result in symmetry breaking of the fields for the active spheres; relative to the non-active spheres, the internal field distributions for the active spheres are by a similar degree for each sphere, and this rotation breaks the left–right symmetry.

3. Application to aggregated particles

Since the primary motivation for this work is to identify the effects of OA particle aggregation on circular polarization, it is appropriate to conclude the paper with a limited set of calculation results pertaining to aggregated particles—with the caveat that the calculations are not intended to represent a comprehensive study of the subject.

Two structural models of aggregates are used in the example calculations: a fractal geometry with D_f=1.8 and k_0=2.2 that is characteristic of aggregates formed from cluster–cluster diffusion processes, and clusters of spheres packed randomly and uniformly into a spherical boundary with a volume fraction of 0.5. This latter form would correspond to aggregates formed from evaporation of the liquid phase from droplets of liquid–solid suspensions. Aggregates for both models were generated for a range of N_S values using a Monte Carlo method. Shown in Fig. 3 are representations of the two types of clusters, with N_S=80.

Orientation-averaged scattering matrix values, for a set aggregate structure model, N_S, and monomer sphere properties, were averaged over 10 pairs of randomly generated realizations of the aggregate. Each aggregate pair consisted of the generated sphere configuration and a mirror-symmetrical version of the configuration. This pairing was done to identically cancel CP effects due to the small yet non-zero chiral geometrical structure of the randomly generated aggregates. Our rationale for employing this contrived scheme is that the sample volume, in an actual measurement, will typically contain a multitude of particles, and barring the existence of some mechanism to produce a preferential orientation and/or a chiral structure in the particles, the geometrical structure of the sample will be statistically isotropic. Consequently, the CP effects seen in our calculations are manifested entirely by optical activity.

For all calculations, the sphere refractive index corresponds to $m_R = 1.55 + 0.0006004i$ and $m_L = 1.5500338 + 0.0006000i$, which are typical for the amino-acids discovered in the Murchison meteorite [10]. According to [11], the specific rotation angle for them is about 100°, which corresponds to a difference in refractive index for left and right circular polarization of 3×10^{-6}.

Shown in Fig. 4 are values of CP=S_{41}/S_{11}, as a function of scattering angle, calculated for the packed sphere configuration. Each curve corresponds to a fixed number of spheres N_S, with N_S ranging from 1 to 128. The plot on the left corresponds to a fixed sphere size parameter of x_S=0.5 for all cases; the solid volume of the cluster will therefore be proportional to N_S. An increasing N_S, for this case, results in CP patterns that evolve in a manner analogous to that for an increasing volume, homogenous OA sphere, i.e., a shift from Rayleigh to resonant behavior.

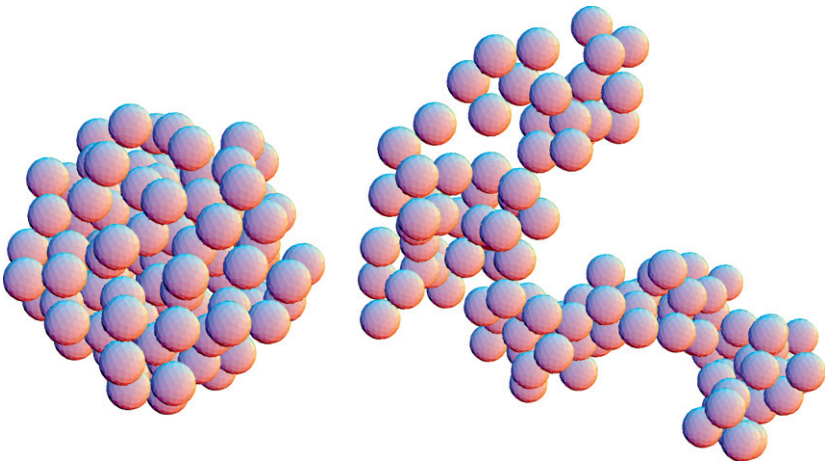

Fig. 3. Packed cluster (left) and fractal aggregate (right).

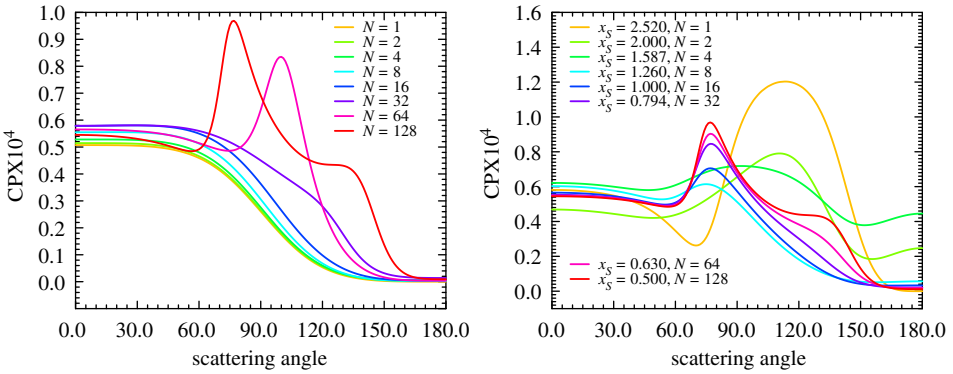

Fig. 4. Circular polarization ratios for the packed cluster. x_S=0.5 (left), x_V=2.52 (right). (For interpretation of the references to color in this figure legend, the reader is referred to the web version of this article.)

The reason that the packed sphere results show the resonance behavior is because the monomers are forced to fit inside a perfect sphere. This effect would wash out if the enclosing boundary was made random, or when averages were made over different N_S. An alternate way at looking at the same effect is shown in the right plot in Fig. 4, for which the solid volume of the cluster is held constant with a corresponding volume-mean size parameter of $x_V=0.5\times 128^{1/3}=2.52$. As N_S increases from 1 to 128 – corresponding to $x_S=2.52\rightarrow 0.5$ – the CP patterns transition from one homogenous limit to another, with the latter corresponding to that predicted by an appropriate mixing rule.

Results for fractal-like aggregates are shown in Fig. 5, with N_S ranging through the same values as before and sphere size parameter x_S=0.5 (left) and 1.0 (right). For the forward scattering directions an increasing N_S results in CP initially increasing to a maximum, followed by a decreasing trend; the latter is most evident in the results for x_S=1. This behavior suggests that the forward-directed CP for fractal aggregates could potentially be modeled using a single appropriate length scale of the aggregate, such as the radius of gyration R_g or the circumscribing sphere radius. Both sets of results also show a significant relative increase in backwards CP with increasing N_S.

The calculation results shown in Fig. 5 are not intended to fit any observational or laboratory data. However, we do see in them some encouraging outcomes. Specifically, the angular change of CP for fractal aggregates with x_S=0.5 is similar to that observed in comets [1], namely within the range of phase angles 20−120° (scattering angles 160–60°) CP increases almost linearly. Though the values of CP are approximately two orders of magnitude smaller than the observed ones (there CP reached 0.4% at the scattering angle 60°), at all angles, except the forward scattering area, the results show increase in the CP with the increase of the number of monomers. We expect that for larger aggregates we may reach higher values of CP. The current models of the cometary dust require domination of particles of thousands of monomers [12]. For such large aggregates, the CP may be significantly larger.

We note again that the curves in Figs. 4 and 5 were generated using a contrived shortcut for configurational averaging; that being the use of mirror-image pairs of aggregate realizations to identically cancel CP effects due to geometrical anisotropy. For a fixed cluster structure model and a fixed N_S, the variability in the calculated CP distribution from one sampled pair to the next was relatively small, and we determined by inspection that

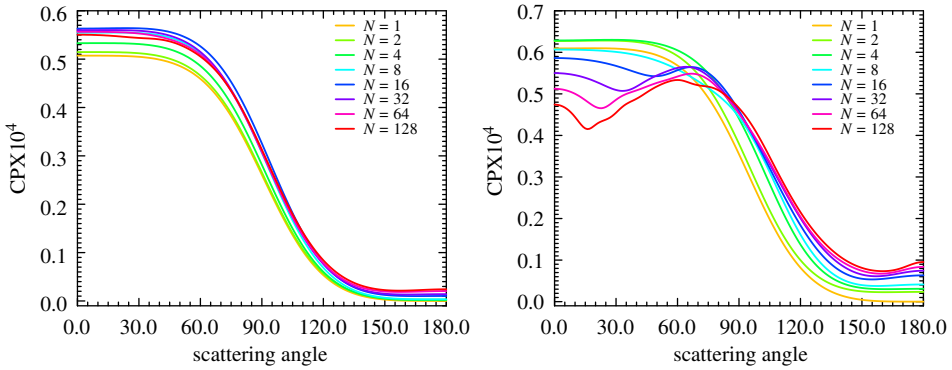

Fig. 5. Circular polarization ratios for the fractal aggregate. x_S=0.5 (left), = 1 (right). (For interpretation of the references to color in this figure legend, the reader is referred to the web version of this article.)

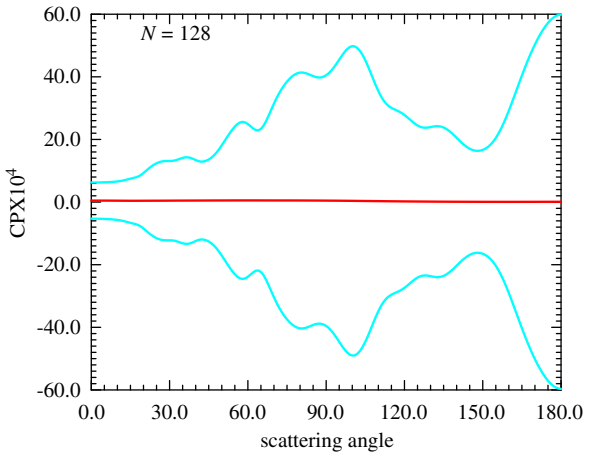

Fig. 6. CP $\pm$ one standard deviation as calculated from 10 random fractal aggregate realizations, x_S=1, N_S=128.

10 sampled pairs provided an accurate estimate of the configurational-averaged behavior. We also expect that the calculated trends in Figs. 4 and 5 are representative of what would be obtained from an averaging scheme that did not employ mirror pairs. However, our calculation results also indicate that the number of non-paired samples required to obtain an accurate average could become huge. This is demonstrated in Fig. 6, where we plot CP $\pm\sigma$ for the x_S=1, fractal aggregate model, where σ is the CP standard deviation calculated from the original 10 (non-paired) random realizations. Shown also in the red curve is the averaged value of CP appearing in Fig. 5. The results indicate that, for the particular L and R refractive index values used in the calculations, CP due to random structural anisotropy in finite N_S aggregates is 10–100 times larger than that due to optical activity. This result could have important implications with regard to measurements; any mechanism which produces a biased, non-random orientation or structure of the aggregate – even as a small, higher-order effect – could potentially create CP comparable with that due to optical activity of the spheres. We plan to examine this and additional issues in future work.

References

[1] Rosenbush V, Kolokolova L, Lazarian A, Shakhovskoy N, Kiselev N. Circular polarization in comets: observations of comet C/1999 S4 (LINEAR) and tentative interpretation. Icarus 2007;186:317–30.
[2] Rosenbush V, Kiselev N, Kolokolova L. Predominantly left-handed circular polarization in comets: does it indicate l-enantiomeric excess in cometary organics? In: Organic matter in space, proceedings of the international astronomical union, IAU symposium, vol. 251; 2008. p. 311–2.
[3] Pizzarello S, Cooper GW. Molecular and chiral analyses of some protein amino acid derivatives in the Murchison and Murray meteorite. Meteoritics Planet Sci 2001;36:897–909.
[4] Sparks WB, Hough JH, Kolokolova L, Germer TA, Chen F, DasSarma S, et al. Circular polarization in scattered light as a possible biomarker. J Quant Spectrosc Radiat Transfer 2009;110:1771–9.
[5] Bohren CF. Scattering of electromagnetic waves by an optically active spherical shell. J Chem Phys 1975;62:1566–71.
[6] Flynn GJ. Physical, chemical, and mineralogical properties of comet 81P/wild 2 particles collected by stardust. Earth Moon Planets 2008;102:447–59.
[7] Bohren CF, Huffman DR. Absorption and scattering of light by small particles. Wiley; 1983.
[8] Mackowski DW, Mishchenko MI. Calculation of the T-matrix and the scattering matrix for ensembles of spheres. J Opt Soc Am A 1996;13:2266–78.
[9] Mackowski DW, Mishchenko MI. A multiple sphere T-matrix FORTRAN code for use on parallel computer clusters. J Quant Spectrosc Radiat Transfer, submitted for publication.
[10] Cronin JR, Pizzarello S. Amino acids in meteorites. Adv Space Res 1983;3:5–18.
[11] Mason SF. Molecular optical activity and the chiral discriminations. Cambridge University Press; 1982.
[12] Kolokolova L, Kimura H, Kiselev N, Rosenbush V. Two different evolutionary types of comets proved by polarimetric and infrared properties of their dust. Astron Astrophys 2007;463:1189–96.